文章编号:1000-0887(2016)12-1296-12

A 3D Compressible Lattice Boltzmann Model and Its Appliaction to Low Mach Number Turbulent Flow*

KUNISHIMA Yuichi, KAJISHIMA Takeo

(*Department of Mechanical Engineering*, *Osaka University*, 2-1 *Yamadaoka*, *Suita*, *Osaka* 565-0871, *Japan*)

Abstract: We intend to improve the finite-difference lattice Boltzmann method (FDLBM) for the use of direct numerical simulation of aerodynamic sound. Using a feature of the LB-based solver, the constant advection velocity in the kinetic equation enables easy implementation of higher-order upwind difference schemes, resulting in high resolutions for sound waves as well as turbulent flow. We release a new particle model which recovers the compressible Navier-Stokes system with flexible specific heat ratio in the 3D space. In addition, we introduce a heat flux modification, which enables us to set Prandtl number freely under the Bhatnagar-Gross-Krook(BGK) collision operator. Our new method performs well in validation problems of weak acoustic waves in a shock tube, and laminar Taylor-Couette flow with a temperature gradient. We conduct a 3D simulation of flow around the NACA0012 aerofoil. The Reynolds number, Mach number and angle of attack are 2×10^5, 8.75×10^{-2} and 9° respectively. Our results are in good agreement with the experimental data about the position of the separation bubble near the leading edge and the Mach number dependence of the surface pressure fluctuation intensity.

Key words: finite-difference lattice Boltzmann method; low Mach number flow; turbulent flow
CLC number: O35; O422 **Document code**: A
doi: 10.21656/1000-0887.370556

Introduction

An advantage of the FDLBM[1] is the constant advection velocity of the discrete Bhatnagar-Gross-Krook (DBGK) equation, which permits easy implementation of higher-order schemes. The FDLBM with a nonlinear higher-order upwind biased scheme achieves high resolution for wall turbulence[2]. It is expected that the FDLBM exhibits good performance for sound waves, and becomes a useful method for analysis of the aerodynamic noise from turbulence. However, the conventional LB-models, D2Q9, D3Q15 and D3Q19, cannot handle thermodynamics of compressible fluid.

Tsutahara et al.[3] conducted direct simulation with the FDLBM and new thermal particle models which can handle the arbitrary specific heat ratio. These models require 42 dis-

* Received 2016-11-08; Revised 2016-11-28
Corresponding author, KUNISHIMA Yuichi, E-mail: kunishima@fluid.mech.eng.osaka-u.ac.jp

tribution functions in the 2D space and 78 in the 3D. Then, a downsized particle model suggested by Kataoka and Tsutahara[4] which recovers the compressible Navier-Stokes system consists of 16 velocities in the 2D space. Though mentioned simultaneously, a definite model with 32 velocities in the 3D space remains veiled today because of its poor numerical performance.

We propose a D3Q32 model and the adjusting method for the Prandtl number. We create a particle velocity set with "rotation" whose degree depends on the specific heat ratio, obtaining sufficient numerical performance for direct simulation of aerodynamic sound in the 3D space. Handling arbitrary Prandtl number with the BGK collision operator, we apply a simple heat flux modification based on "Prandtl number fix" of Xu's BGK scheme[5].

Two validation tests are conducted with the D3Q32 model. We confirm the speed of sound and invest the executable temperature range in a shock tube test of weak acoustic waves[3]. The laminar Taylor-Couette flow with a temperature gradient is implemented to confirm the Prandtl number modification from the viewpoint of isotropic diffusion and Galilean invariance. We finally apply the model to flow around the NACA0012 aerofoil at moderate Reynolds numbers[6] to survey the capability in direct simulation of aerodynamic sound at low Mach numbers.

The rest of this paper is organized as follows. Section 1 provides our numerical modelling in detail. Results of the 2 validation problems are reported in section 2. Numerical results of the NACA aerofoil problem are shown and compared with the experimental and numerical data[7] in section 3. Section 4 presents our conclusions.

1 Methodology

1.1 Governing equation

The governing equation of the finite-difference lattice Boltzmann method[3] is

$$\frac{\partial f_m}{\partial t} + c_{mi}\frac{\partial g_m}{\partial x_i} = \frac{f_m^{\mathrm{eq}} - f_m}{\phi}, \tag{1}$$

where t is the time and $x_i (i = 1,2,3)$ is the Cartesian coordinate; c_{mi} is the particle velocity of the m-th particle, f_m is the distribution function; f_m^{eq} is the local equilibrium distribution function and ϕ is the relaxation time; and g_m is the modified distribution function defined as follows:

$$g_m|_{\mathrm{org}} := \left(1 - \frac{a}{\phi}\right) f_m + \frac{a}{\phi} f_m^{\mathrm{eq}}, \tag{2}$$

where a is the modified coefficient which adjusts relation between ϕ and diffusion coefficients in the macroscopic system[8], and $|_{\mathrm{org}}$ is the precaution against redefinition in the Prandtl number fix (seen in subsection 1.5).

1.2 Compressible Navier-Stokes system

Our compressible lattice Boltzmann model aims at the compressible Navier-Stokes (NS) system:

$$\frac{\partial \rho}{\partial t} + \frac{\partial \rho u_i}{\partial x_i} = 0, \tag{3}$$

$$\frac{\partial \rho u_i}{\partial t} + \frac{\partial \rho u_i u_j}{\partial x_j} + \frac{\partial p}{\partial x_i} = -\frac{\partial P'_{ij}}{\partial x_j}, \tag{4}$$

$$\frac{\partial \rho e}{\partial t} + \frac{\partial (\rho e + p) u_i}{\partial x_i} = \frac{\partial}{\partial x_j}\left(\lambda \frac{\partial T}{\partial x_j} - P'_{ij} u_i\right), \tag{5}$$

where ρ, u_i, and T are the density, velocity, and temperature respectively; e is the total energy per unit mass written in eq.(6), and p is the pressure determined by the equation of state (eq.(7)); and P'_{ij} is the viscous stress tensor defined in eq.(8), and λ is the thermal conductivity,

$$e = \frac{b}{2} T + \frac{u_k^2}{2}, \tag{6}$$

$$p = \rho T, \tag{7}$$

$$P'_{ij} := -\mu\left(\frac{\partial u_j}{\partial x_i} + \frac{\partial u_i}{\partial x_j} - \frac{2}{3}\frac{\partial u_k}{\partial x_k}\delta_{ij}\right) - \mu_B \frac{\partial u_k}{\partial x_k}\delta_{ij}, \tag{8}$$

where b in eq.(6) is the internal degree of freedom, which determines specific heat ratio γ written in eq.(9); and μ, μ_B in eq.(8) are the shear viscosity and the bulk viscosity,

$$\gamma = \frac{b+2}{b}. \tag{9}$$

It is noted that we handle dimensionless values and gas constant is set to 1 in this paper.

Table 1 The particle velocity set of D3Q32

m	translation c_{mi}	rotation η_m
1~6	(±2,0,0) cyc	0
7~12	(±2,0,0) cyc	2
13~24	(±2,±2,0) cyc	0
25~32	(±1,±1,±1)	$\sqrt{b-3}$

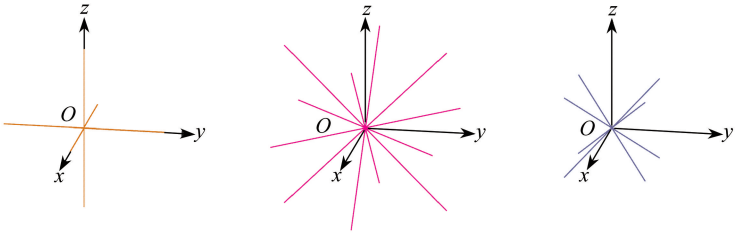

(a) m = 1 ~ 12 (b) m = 13 ~ 24 (c) m = 25 ~ 32

Fig. 1 Schematics of the the particle velocity set

1.3 Macroscopic variables and local equilibrium distribution function

Macroscopic variables are defined by the distribution function as

$$\rho := \sum\nolimits_m f_m, \quad u_i := \frac{1}{\rho}\sum\nolimits_m f_m c_{mi}, \quad e := \frac{1}{\rho}\sum\nolimits_m f_m \frac{c_{mi}^2 + \eta_m^2}{2}, \tag{10a~c}$$

and the local equilibrium distribution function is given by

$$f_m^{\mathrm{eq}} := \rho\left[A_m + B_m c_{mi} u_i + D_m c_{mi} c_{mj} u_i u_j + E_m c_{mi} c_{mj} c_{mk} u_i u_j u_k\right], \tag{11}$$

where A_m, B_m, D_m and E_m are the model coefficients. The forms of them are identical to those of the 2D model by Kataoka and Tsutahara[4].

The constraints for f_m^{eq} to recover the NS system in eq.(1) are

$$\sum_m f_m^{\mathrm{eq}} = \rho,\ \sum_m f_m^{\mathrm{eq}} c_{mi} = \rho u_i, \tag{12a,b}$$

$$\sum_m f_m^{\mathrm{eq}} c_{mi} c_{mj} = \rho u_i u_j + p\delta_{ij},\ \sum_m f_m^{\mathrm{eq}} \frac{c_{mi}^2 + \eta_m^2}{2} = \rho e, \tag{12c,d}$$

$$\sum_m f_m^{\mathrm{eq}} c_{mi} c_{mj} c_{mk} = p(u_i\delta_{jk} + u_j\delta_{ki} + u_k\delta_{ij}) + \rho u_i u_j u_k, \tag{12e}$$

$$\sum_m f_m^{\mathrm{eq}} c_{mi} \frac{c_{mj}^2 + \eta_m^2}{2} = (\rho e + p) u_i, \tag{12f}$$

$$\sum_m f_m^{\mathrm{eq}} c_{mi} c_{mj} \frac{c_{mk}^2 + \eta_m^2}{2} = T(\rho e + p)\delta_{ij} + (\rho e + 2p) u_i u_j. \tag{12g}$$

Under these constraints, μ, μ_{B} and λ are settled as eqs.(13a~c), which indicate $Pr \equiv 1$.

$$\mu = p(\phi - a),\ \mu_{\mathrm{B}} = \left(\frac{2}{3} - \frac{2}{b}\right) p(\phi - a),\ \lambda = \frac{b+2}{2} p(\phi - a). \tag{13a~c}$$

1.4 Particle velocity set of D3Q32 model

We determine particle velocities as shown in table 1. The velocity set with the 2 sublattices ($m = 13 \sim 24$ and $m = 25 \sim 32$) shown in fig. 1 is needed to recover the compressible NS system. From this, we use x, y, z along with x_1, x_2, x_3. The rotational speed for $m = 25 \sim 32$, parameterized by b, gives us good numerical performance especially in isotropy of diffusion. The same velocities for $m = 1 \sim 6$ and $m = 7 \sim 12$ are settled for the convenience of the Prandtl number fix (seen in subsection 1.5).

Once determining the particle velocity set, we can concrete A_m, B_m, D_m and E_m in eq.(11) automatically and uniquely:

$$A_{1\sim6} = -1 + \frac{b+8}{8} T + -\frac{1}{8} G + \left(\frac{3}{8} - \frac{1}{32} H\right) u_i^2, \tag{14a}$$

$$A_{7\sim12} = -\frac{4b+12}{3(8-b)} + \frac{3b^2 + 23b - 96}{24(8-b)} T - \frac{b-3}{8(8-b)} G + \left(\frac{21b-56}{48(8-b)} - \frac{b-2}{32(8-b)} H\right) u_i^2, \tag{14b}$$

$$A_{13\sim24} = \frac{4b - 7bT + 3G - 4u_i^2}{48(8-b)}, \tag{14c}$$

$$A_{25\sim32} = \frac{64 - (8b+48) T + 6G - (32 - 3H) u_i^2}{16(8-b)}, \tag{14d}$$

$$B_{1\sim6} = \frac{b-2}{24} - \frac{b-3}{16} T - \frac{1}{32} u_i^2, \tag{15a}$$

$$B_{7\sim12} = -\frac{b-3}{24} + \frac{b-3}{16} T, \tag{15b}$$

$$B_{13\sim24} = -\frac{1}{48} + \frac{1}{32} T, \tag{15c}$$

$$B_{25\sim32} = \frac{1}{6} - \frac{1}{8}T - \frac{1}{16}u_i^2, \tag{15d}$$

$$D_{1\sim6} = \frac{8-H}{128},\ D_{7\sim12} = \frac{3b-16}{64(8-b)} - \frac{b-6}{128(8-b)}H, \tag{16a,b}$$

$$D_{13\sim24} = -\frac{b-H}{128(8-b)},\ D_{25\sim32} = \frac{8-H}{16(8-b)}, \tag{16c,d}$$

$$E_{1\sim6} = \frac{8-b}{384},\ E_{7\sim12} = \frac{b-3}{384},\ E_{13\sim24} = \frac{1}{768},\ E_{25\sim32} = \frac{1}{48}, \tag{17a~d}$$

where G and H are defined in eqs.(18a, b) for simplicity. Though a restriction, $b < 8$, that is $\gamma > 1.25$, is imposed from those coefficients, the value of the air is still in range,

$$G := T((b+2)T + u_i^2),\ H := (b+4)T + u_i^2. \tag{18a, b}$$

1.5 Prandtl number fix in FDLBM

Applying the Prandtl number fix of Xu's BGK scheme[5], we introduce a practical procedure for the arbitrary Prandtl number in the FDLBM. He derived a heat flux with the BGK collision operator from an integral of the distribution function, multiplied the flux by $(1/Pr - 1)$, and added it to the energy equation. This method prevents 2 probable difficulties. One is dilatation of computational time in the multi-relaxation time[9] or a further realistic collision operator. The other is dependence on accuracy of the viscous term to the resolution of wall turbulence[10] from an extra temperature differential term.

By introducing Xu's procedure into the FDLBM, heat flux h_i can be derived from summation instead of integration. Watching the effect of modified coefficient a, we define h_i as

$$h_i := \left(1 - \frac{a}{\phi}\right)\sum_m f_m(c_{mi} - u_i)\frac{(c_{mj} - u_j)^2 + \eta_m^2}{2}. \tag{19}$$

It is noted that h_i in the D3Q32 model can recover the heat flux at the unit Prandtl number, that is

$$h_i = \frac{b+2}{2}\mu\frac{\partial T}{\partial x_i} + O(\phi). \tag{20}$$

Then, we re-modify the advection term of eq.(1) to

$$g_m := \left(1 - \frac{a}{\phi}\right)\left[f_m + \left(\frac{1}{Pr} - 1\right)W_m c_{mj} h_j\right] + \frac{a}{\phi}f_m^{\mathrm{eq}}, \tag{21}$$

where W_m are the weighting coefficients which satisfy the constraints as follows:

$$\sum_m W_m c_{mi} c_{mj} = 0,\ \sum_m W_m c_{mi} c_{mj} c_{mk} = 0,\ \sum_m W_m c_{mi} c_{mj}(c_{mk}^2 + \eta_m^2) = \delta_{ij}. \tag{22a~c}$$

Equations(23a~c) mean the additional term modifies the energy flux and doesn't affect the mass and momentum fluxes. We determine W_m in eqs.(23a~c) from a viewpoint of computational efficiency,

$$W_{1\sim6} = -\frac{1}{32},\ W_{7\sim12} = \frac{1}{32},\ W_{13\sim32} = 0. \tag{23a~c}$$

1.6 Discretization schemes

Finally, we briefly explain the discretization schemes for eq.(1). Ketcheson's explicit 4th-order 2-storage Runge-Kutta scheme[11] is used for time integration. For space differen-

tiation, the 3rd-order upwind compact scheme is chosen for validation problems to exclude numerical instability of the scheme, and the higher-order nonlinear upwind biased scheme[2] is applied for an application problem due to its high performance in turbulent flow.

$\rho_1 = 1.0 + 1\times10^{-6}$	$\rho_2 = 1.0$
$u_1 = 0$	$u_2 = 0$
$T_1 = T_0$	$T_2 = T_0$

Fig. 2 Initial conditions in the shock tube

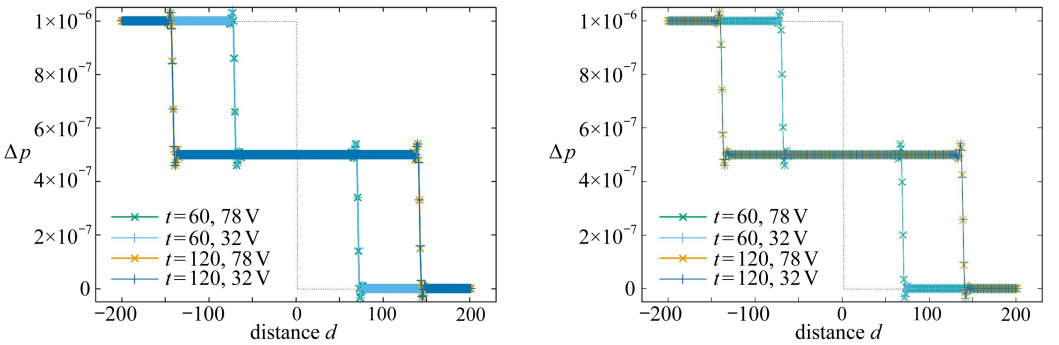

(a) $\gamma = 1.4$, $T_0 = 1.0$ (b) $\gamma = 4/3$, $T_0 = 1.0$

Fig. 3 Pressure variation profiles (the present scheme (32 V) agrees well with the conventional model (78 V) at various γ values)

2 Validation

2.1 Weak acoustic waves in shock tube

We conduct a numerical test of weak acoustic waves in a shock tube[3] to validate the sound speed of the D3Q32 model. The relation between the speed of sound and the particle velocities varying with the temperature and the stable range of temperature is also investigated.

The initial conditions are shown in fig. 2. The parameters are specific heat ratio γ, and initial temperature T_0. We prepare the 1D grid which is along the x-direction in fig. 1 with unit intervals, and set the time step to 0.8. Both ϕ and a are set to $0.1\dot{3}$ for inoperativeness of the diffusion and computational efficiency of the collision process.

The pressure profiles at different γ values are shown in fig. 3. The present results (32 V) show excellent agreement with those of the conventional 3D FDLBM (78 V)[3]. And then, our model is stable for $T_0 \in [0.7, 1.4]$ at $\gamma = 1.4$; still, the instability on the lower temperature side is not seen in the conventional model. The D3Q32 model achieves the arbitrary specific heat ratio with less than half number of distribution functions of the conventional model. And, it is sufficient for most of subsonic flows to be executable in distribution with double temperature ratios.

2.2 Laminar Taylor-Couette flow with temperature gradient

We validate the Prandtl number fix in the laminar Taylor-Couette flow with the 3-step

Prandtl numbers, 0.72, 1.0 and 2.5 from the viewpoint of isotropy and Galilean invariance. The computational domain is described in fig. 4. We set $R_1 = 1.5L$ and $R_2 = 2.5L$. Just the inner cylinder is rotated with angular velocity $U/(2\pi R_1)$. Reynolds number $\rho UL/\mu$ is set to 100 for laminar solution, the Mach number for U is set to 0.1, and the specific heat ratio is 1.4 as the value of the air. The nonslip and isothermal boundary condition is applied on the cylinder surfaces, where the ratio of the outer/inner temperature is set to $(1-1/(1.4\times 10^4))$.

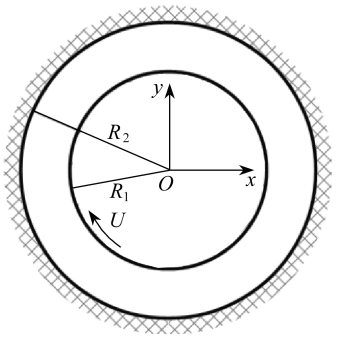

Fig. 4 The Taylor-Couette flow

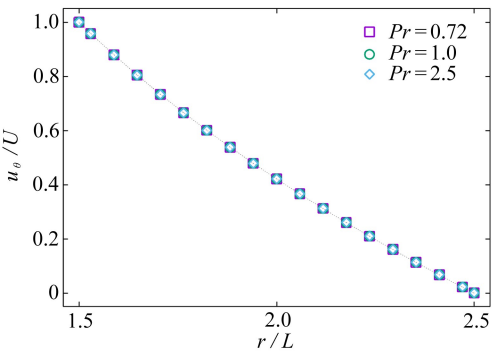

(a) The circumferential velocity

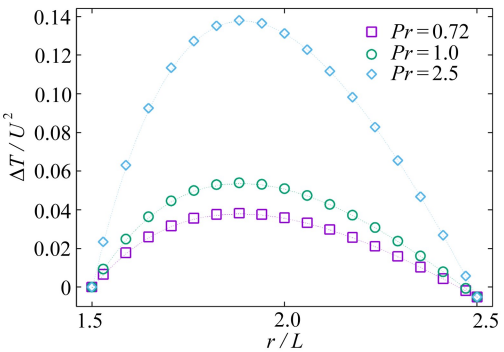

(b) The temperature difference

Fig. 5 Steady solutions for $x \in [-2.5, -1.5]$, $y = 1$ at various Prandtl numbers for $|V_i| = 0$ (all results agree with the theoretical profiles)

Table 2 The numerical setup for the NACA0012 simulation

parameter	value
specific heat ratio γ	1.4
temperature T_0	0.9
Reynolds number based on chord length Re_C	2.0×10^5
Mach number Ma	8.75×10^{-2}
Prandtl number Pr	0.72
angle of attack θ_{AOA}/(°)	9
number of grid points	594/139/192
grid width of first layer on aerofoil Δ_{min}	$\cong 8.69\times10^{-5}L_C$
spanwise grid width Δz	$5.0\times10^{-3}L_C$
time step Δt	$\cong 8.69\times10^{-5}$
modified coefficient a	$\cong 1.45\times10^{-5}$
relaxation time ϕ	$\cong 1.50\times10^{-5}$

We provide temperature at inner boundary 0.9 which works best; thus, the reference sound speed is about 1.12. For the sake of the unit reference pressure, the reference density is set to 10/9. We handle a plane perpendicular to the z-direction in fig. 1, and prepare the polar grid with 75/17 points along the circumferential/radial direction. The minimum grid width is about 5.77×10^{-2}, and we set the time step to about 4.61×10^{-2}. As a result, the advantageous value of a is about 7.69×10^{-3}, and ϕ is obtained as 8.94×10^{-3}.

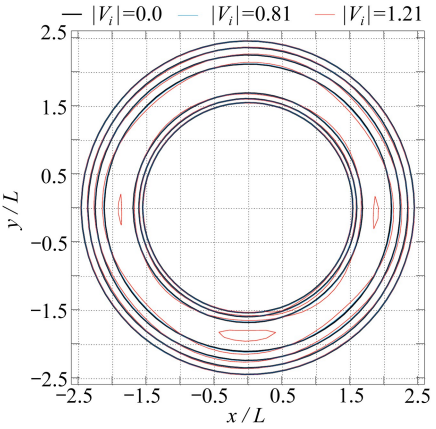

Fig. 6 Isolines of 6 levels from $T_{\min}$ to $T_{\max}$ for $Pr = 0.72$ (isotropic profiles keep for $|V_i| = 0.0, 0.81$)

Grid velocity V_i to confirm the Galilean invariance of the procedure is introduced into eq.(1) as follows:

$$\frac{\partial f_m}{\partial t} + (c_{mi} - V_i)\frac{\partial g_m}{\partial x_i} = \frac{f_m^{\mathrm{eq}} - f_m}{\phi}, \tag{24}$$

which is terser than the previous arbitrary Lagrangian Eulerian formulation[12]. The difference becomes $O(\phi^2)$, and no significant effect is taken into the recovery of the NS system. We determine $|V_i|$ as 0.0, 0.81 and 1.21 under the given condition $3V_1 = 4V_2$. The initial condition is steady with the reference density and temperature. The number of time steps is about 21 000 to reach stable solutions.

Profiles along the radial direction at various Prandtl numbers for $|V_i| = 0$ are shown in fig. 5. All results agree with the theoretical profiles, and the Prandtl number fix works successfully. It is noted that the theoretical values are derived with the constant diffusion coefficients in spite of the proportion to temperature in the FDLBM. Fig. 6 shows the temperature profiles for $Pr = 0.72$. We can see isotropy for $|V_i| = 0, 0.81$. These results show the reasonable performance of our model, and the distortion for $|V_i| = 1.21$ is out of our control because the grid velocity almost reaches the particle velocities. It is concluded that the Prandtl number fix enables us to handle the value of the air.

3 Application to flow around NACA0012 aerofoil at moderate Reynolds number

3.1 Aim and numerical setup

We conduct a simulation of flow around the NACA0012 aerofoil. We validate reproduc-

ibility of our method from the viewpoint of capability for direct simulation of aerodynamic sound. The statistic values on the surface of the aerofoil are compared with experimental and numerical data by Miyazawa et al.[7]. We validate the Reynolds number effect, separation and reattachment, and the Mach number dependence around the aerofoil[13].

We define x - and z -directions as chordwise and spanwise, then set y -direction orthogonal to them. The C-type structural grid with uniform spanwise grid widths is prepared. The parameters are written in table 2, where L_C represents the chord length and the first/last value of the number of grid corresponding to the circumferential/spanwise directions.

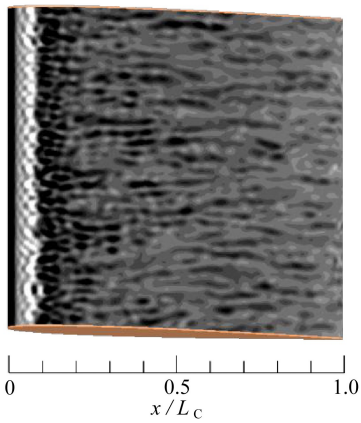

Fig. 7 Distribution of instantaneous spanwise vorticity ω_z on the suction surface: $\omega_z \in [-500, 500]$ where the uniform velocity is used as the reference velocity

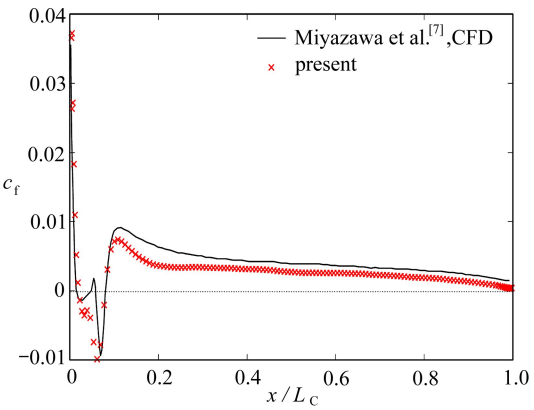

Fig. 8 Friction coefficient c_f on the suction surface

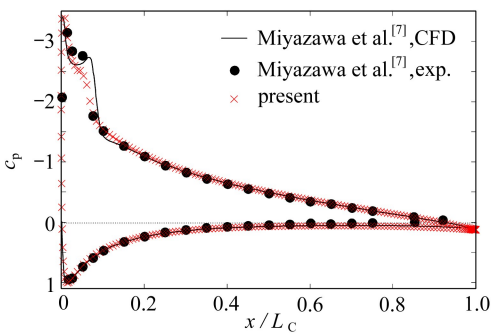

Fig. 9 Mean pressure coefficient c_p on the surface

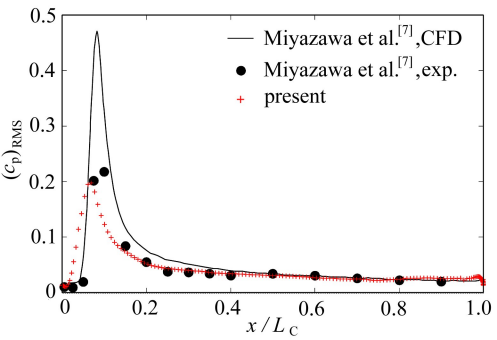

Fig. 10 Intensity of pressure fluctuation $(c_p)_{RMS}$ on the suction side

3.2 Results and discussion

The instantaneous z -direction vorticity field on the suction side is described in fig. 7, where positive/negative values correspond to white/black. We can see the reverse-flow region near the leading edge $0.03L_C \leqslant x \leqslant 0.09L_C$. The separation bubble which is considered as a major sound source[7] has a quasi-periodic structure along the spanwise direction. The result suggests the 3D computation is necessary to capture sound source and to predict

sound emission.

Fig. 8 shows friction coefficient c_f obtained by eqs. (25a~c)[2], where c_n/c_l represents the normal/tangential direction of the surface. The separation and reattachment point of our results agrees well with the previous numerical results[7], with finer grid resolution. It can be stated that the FDLBM has a capability to treat viscous effect with computational efficiency.

$$P'_{nl} := \left(1 - \frac{a}{\phi}\right) \sum_m (f_m - f_m^{eq}) c_n c_l , \tag{25a}$$

$$c_f := P'_{nl} \Big/ \left(\frac{1}{2}\rho U^2\right) , \tag{25b}$$

$$c_p := (p - p_0) \Big/ \left(\frac{1}{2}\rho U^2\right) . \tag{25c}$$

The profile of pressure coefficient c_p defined in eqs.(25a~c) also agrees with the previous experimental and numerical results (fig. 9). In addition to importance of the average of c_p in aerodynamics, its variation is essential in aeroacoustics. It is reported that the pressure fluctuation near the separation point intensifies as the Mach number decreases[13]. Our method can reproduce the the Mach number dependence (fig. 10); in contrast, the previous computation overestimates the peak value due to the incompressible treatment.

Our results reproduce the position of the separation bubble near the leading edge and the pressure fluctuation on the suction side in the previous experimental and numerical ones. These results mean that the viscous and compressible effects in the flow are handled correctly.

4 Conclusions

A new compressible model of the finite-difference lattice Boltzmann method is investigated to utilize its advantage in direct simulation of aerodynamic sound. The new model replaces a feasible compressible FDLBM in the 3D space with less than half number of distribution functions of the conventional model, and releases us from the restrictions about the specific heat ratio and the Prandtl number. Our model can handle the properties of the compressible Navier-Stokes system. Furthermore, the Reynolds number and Mach number effects in the flow around the NACA0012 aerofoil are reproduced. Our scheme is a hopeful method for direct simulation of aerodynamic sound of low Mach turbulent flow in the 3D space.

References:

[1] CAO Nian-zheng, CHEN Shi-yi, JIN Shi, Martínez D. Physical symmetry and lattice symmetry in the lattice Boltzmann method[J]. *Physical Review E*, 1997, **55**(1): R21-R24.

[2] Kunishima Y, Kajishima T, Tsutahara M. Higher-order non-linear scheme of finite-difference

lattice Boltzmann method (evaluation by direct numerical simulation of turbulent channel flow)[J]. *Transactions of the JSME*, 2016, **82**(840): 16-00204. doi: 10.1299/transjsme.16-00204. (in Japanese)

[3] Tsutahara M, Kataoka T, Shikata K, Takada N. New model and scheme for compressible fluids of the finite difference lattice Boltzmann method and direct simulations of aerodynamic sound[J]. *Computers & Fluids*, 2008, **37**(1): 79-89.

[4] Kataoka T, Tsutahara M. Lattice Boltzmann model for the compressible Navier-Stokes equations with flexible specific-heat ratio[J]. *Physical Review E*, 2004, **69**(3): 035701. doi: 10.1103/PhysRevE.69.035701.

[5] XU Kun. A gas-kinetic BGK scheme for the Navier-Stokes equations and its connection with artificial dissipation and Godunov method[J]. *Journal of Computational Physics*, 2001, **171**(1): 289-335.

[6] Tam C K W, JU Hong-bin. Aerofoil tones at moderate Reynolds number[J]. *Journal of Fluid Mechanics*, 2012, **690**: 536-570.

[7] Miyazawa M, Kato C, Suzuki Y, Takaishi T. Aeroacoustic simulation of a flow around a 2-D aerofoil (1st report, validation of a large eddy simulation of separated and transitional flow around an aerofoil)[J]. *Transactions of the Japan Society of Mechanical Engineers* (*Series B*), 2006, **72**(721): 2140-2147. (in Japanese)

[8] Tsutahara M, Kurita M, Iwagami T. A study of new finite difference lattice Boltzmann model [J]. *Transactions of the Japan Society of Mechanical Engineers* (*Series B*), 2002, **68**(665): 15-21.

[9] Tamura A, Okuyama K, Takahashi S, Ohtsuka M. Three-dimensional discrete-velocity BGK model for the incompressible Navier-Stokes equations[J]. *Computers & Fluids*, 2011, **40**(1): 149-155.

[10] Suzuki H, Nagata K, Sakai Y, Hayase T, Hasegawa Y, Ushijima T. An attempt to improve accuracy of higher-order statistics and spectra in direct numerical simulation of incompressible wall turbulence by using the compact schemes for viscous terms[J]. *International Journal for Numerical Methods in Fluids*, 2013, **73**(6): 509-522.

[11] Ketcheson D I. Highly efficient strong stability-preserving Runge-Kutta methods with low-storage implementations[J]. *SIAM Journal on Scientific Computing*, 2008, **30**(4): 2113-2136.

[12] Tamura A, Tsutahara M. Simulation of flows and acoustic field around moving body by ALE formulation in finite difference lattice Boltzmann method[J]. *Journal of Environment and Engineering*, 2007, **2**(3): 458-469.

[13] Han C, Kajishima T. Large eddy simulation of weakly compressible turbulent flow around an airfoil[J]. *Journal of Fluid Science and Technology*, 2014, **9**(4): JFST0063. doi: 10.1299/jfst.2014jfst0063.

三维可压缩 Boltzmann 模型及其在低 Mach 数湍流中的应用

国岛雄一, 梶岛岳夫

(大阪大学 机械工程系学院, 大阪 吹田 山田丘 2-1 565-0871, 日本)

摘要: 改进了有限差分格子 Boltzmann 方法(FDLBM),以直接数值模拟气动噪声.基于 LB 求解器特性,采用动力学方程中的恒定对流速度以实施高阶迎风差分,提高了声波和湍流的分辨率.通过建立一个新的三维粒子模型,计算得到了任意比热容的三维可压缩 Navier-Stokes 系统.此外,利用 Bhatnagar-Gross-Krook(BGK)碰撞算子,通过引入热流量修正,实现了 Prandtl 数的可变性.在激波管内弱声波以及伴随有温度梯度的 Taylor-Couette 层流的验证计算中,提出的新方法结果良好.此外也对 NACA0012 翼型绕流进行了三维模拟.其中,Reynolds 数、Mach 数和攻角分别取 2×10^5, 8.75×10^{-2} 以及 9°.计算发现,在机翼前缘附近的分离气流位置,以及表面压力波动强度的 Mach 数依赖性方面,数值计算结果与实验结果相吻合.

关 键 词: 有限差分格子 Boltzmann 方法; 低 Mach 数流动; 湍流

引用本文/Cite this paper:

KUNISHIMA Yuichi, KAJISHIMA Takeo. A 3D compressible lattice Boltzmann model and its appliaction to low Mach number turbulent flow[J]. *Applied Mathematics and Mechanics*, 2016, **37**(12): 1296-1307.

国岛雄一, 梶岛岳夫. 三维可压缩 Boltzmann 模型及其在低 Mach 数湍流中的应用[J]. 应用数学和力学, 2016, **37**(12): 1296-1307.